

Ultrasensitive gas detection of large-area boron-doped graphene

Ruitao Lv^{a,b,c,1}, Gugang Chen^{d,1}, Qing Li^{e,1}, Amber McCreary^{b,c,1}, Andrés Botello-Méndez^{f,1}, S. V. Morozov^g, Liangbo Liang^h, Xavier Declerck^f, Nestor Perea-López^{b,c}, David A. Cullenⁱ, Simin Feng^{b,c}, Ana Laura Elías^{b,c}, Rodolfo Cruz-Silva^j, Kazunori Fujisawa^{b,c}, Morinobu Endo^j, Feiyu Kang^a, Jean-Christophe Charlier^f, Vincent Meunier^h, Minghu Pan^k, Avetik R. Harutyunyan^d, Konstantin S. Novoselov^g, and Mauricio Terrones^{b,c,j,l,m,2}

^aKey Laboratory of Advanced Materials of Ministry of Education of China, School of Materials Science and Engineering, Tsinghua University, Beijing, 100084, China; ^bDepartment of Physics, The Pennsylvania State University, University Park, PA 16802, USA; ^cCenter for 2-Dimensional and Layered Materials, The Pennsylvania State University, University Park, PA 16802, USA; ^dHonda Research Institute USA Inc., 1381 Kinnear Road, Columbus, Ohio 43212, USA; ^eInstitute of Functional Nano and Soft Materials, Soochow University, Suzhou 215123, P. R. China; ^fInstitute of Condensed Matter and Nanosciences, Université catholique de Louvain, 1348 Louvain-la-Neuve, Belgium; ^gSchool of Physics & Astronomy, University of Manchester, Manchester, M13 9PL, UK; ^hDepartment of Physics, Applied Physics and Astronomy, Rensselaer Polytechnic Institute, Troy, New York 12180, USA; ⁱMaterials Science & Technology Division, Oak Ridge National Laboratory, Oak Ridge, TN 37831, USA; ^jResearch Center for Exotic Nanocarbons, Shinshu University, Wakasato 4-17-1, Nagano-city 380-8553, Japan; ^kSchool of Physics, Huazhong University of Science and Technology, Wuhan 430074, China; ^lDepartment of Chemistry, The Pennsylvania State University, University Park, PA 16802, USA; and ^mDepartment of Materials Science & Engineering, The Pennsylvania State University, University Park, PA 16802, USA

¹R.L., G.C., Q.L., A.M. and A.B.M. contributed equally to this work.

²To whom correspondence may be addressed. E-mail: mut11@psu.edu.

(1) Synthesis of B-doped graphene (BG) sheets

The synthesis of large-area BG sheets was achieved in a bubbler-assisted chemical vapor deposition (BA-CVD) system, which is demonstrated in Fig. S1. A typical run for BG synthesis can be described as follows. Firstly, copper foils (99.8% purity, 25 μm thick, Alfa Aesar) were cleaned in a diluted HCl aqueous solution (HCl:H₂O=1:3 v/v), dried with N₂ airbrush and then loaded into the quartz tubing reactor. Before heating the reactor up, a mixture of Ar (1000 sccm) and H₂ (50 sccm) was introduced into the reactor to degas the air inside. Subsequently, the reactor was heated up to 1000 °C with the steps shown in Fig. S2 and kept constant for 10 min in order to anneal the copper foils. After that, a 0.5 M triethylborane (TEB)/hexane solution was bubbled with 1 sccm Ar into the reactor at 1000 °C for 5 min. Finally, the reactor was cooled down to room temperature in an Ar flow. The copper foils with BG sheets were taken out of the reactor for further characterizations. Pristine graphene (PG) sheets were synthesized by using only hexane as precursor.

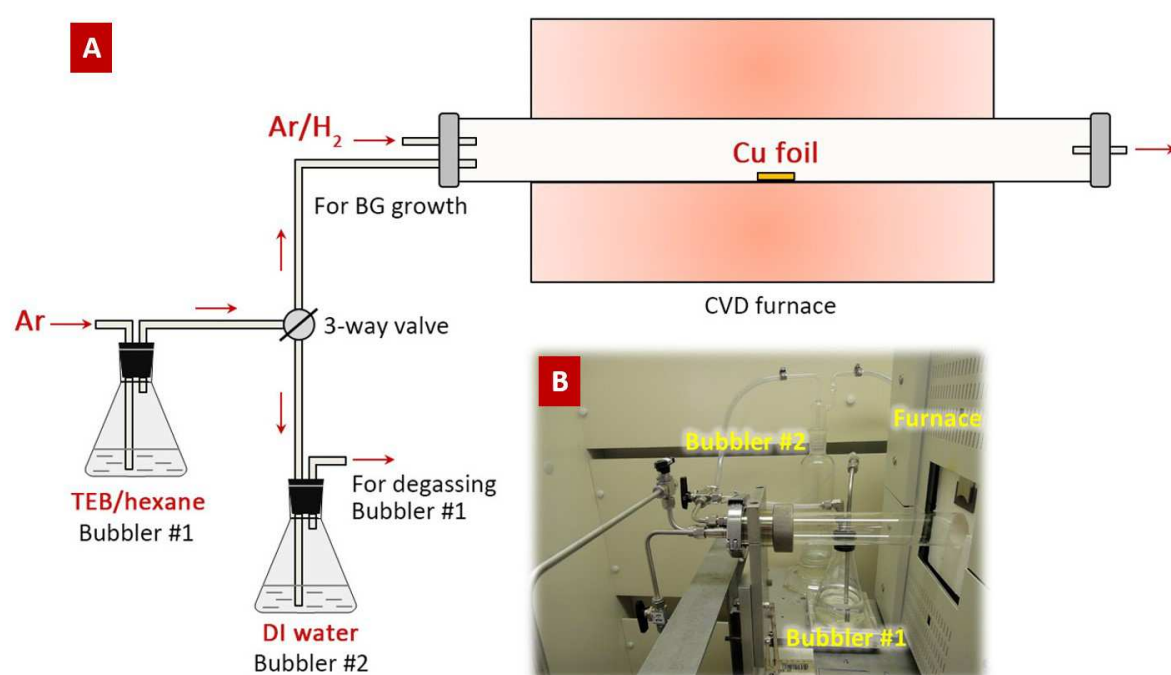


Fig. S1. Ambient-pressure chemical vapor deposition (AP-CVD) setup for the synthesis of B-doped graphene (BG) sheets. (A) Schematic diagram and (B) a photograph of the inlet part of the experimental setup. Here TEB and DI water denote triethylborane and deionized water, respectively.

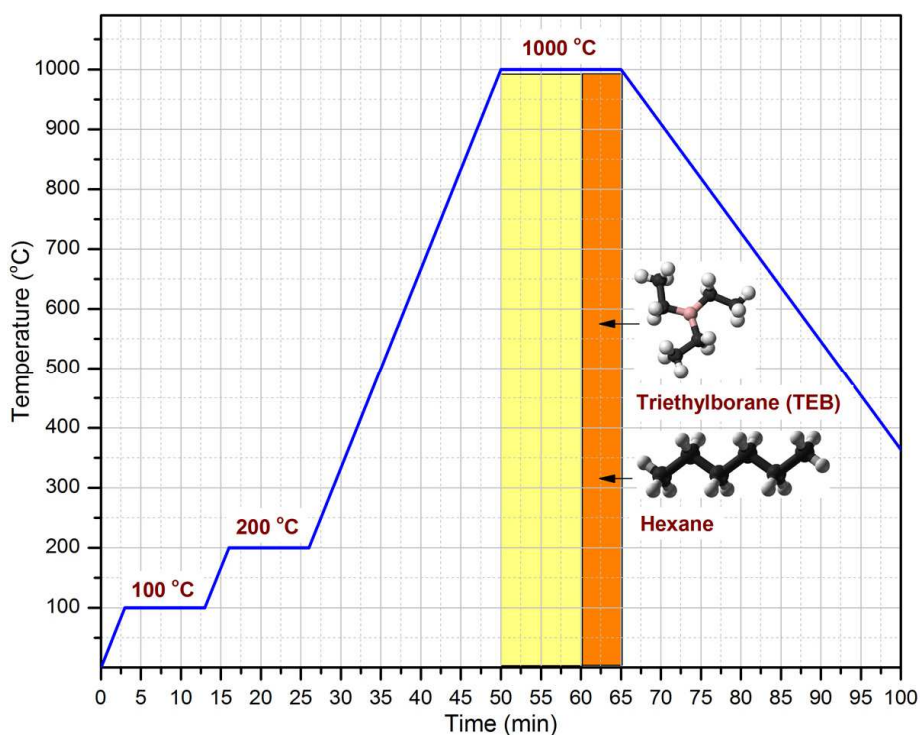


Fig. S2. Heating curves for synthesis of B-doped graphene (BG) sheets. At 1000 °C, the temperature will be kept constant for 10 min in order to anneal the copper foils. After that, a 0.5 M triethylborane (TEB)/hexane solution was bubbled with 5 sccm Ar into the reactor for 5 min.

(2) Transfer BG sheets onto other substrates

As-grown BG sheets were on copper foils (Fig. S3A). In order to carry out further characterization, they were transferred onto other substrates (e.g. silicon wafers, quartz slides, TEM grids). For large-area transfer onto silicon wafers (Fig. S3B) or quartz slides (Fig. S3C), poly(methyl methacrylate) (PMMA) was used as a protective layer. Typically, the top surface of BG sheets was firstly coated with PMMA by spin coating at 4000 rpm for 60 s. Then, Cu foil underneath the BG sheet was etched away in copper etchant (FeCl_3/HCl (0.5 M/0.5 M) aqueous solution in present work) at 50 °C. Next, PMMA/BG sheets were rinsed several times in deionized water to remove the FeCl_3 residues. Afterwards, a piece of SiO_2/Si wafer (or quartz slide) was used to fish the floating PMMA/BG sheets from deionized water. Finally, PMMA was removed from the top surface of BG sheets by alternative rinse in acetone (10 s) and isopropanol (10 s) solvents for 2 min. A high-quality, large-area BG sheet could thus be obtained on SiO_2/Si wafer after blowing solvents away with compressed N_2 .

In the case of transferring BG sheets onto Au TEM grid, a polymer-free method based on the work of Zettl group was used (1). Firstly, TEM grid was mounted onto a piece of copper foil with BG sheet. Then, a drop of IPA was used to bind the amorphous carbon (*a*-C) layer of TEM grid and the BG sheet by surface tension. After the IPA was evaporated away, the *a*-C and BG sheet could combine tightly. Next, Cu foil underneath the BG sheet was etched away. BG sheets on TEM grid could finally be obtained after water rinse and drying. The sample could then be analyzed by high-resolution transmission electron microscopy (HRTEM). Some scanning electron microscopy (SEM) images of BG sheets on Au TEM grid can be seen in Fig. S3D-G.

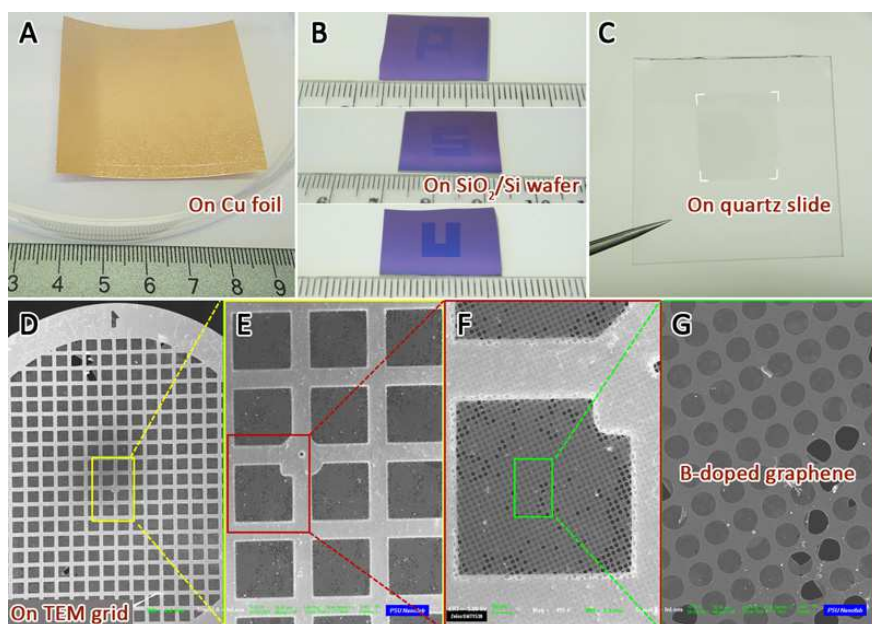


Fig. S3. BG sheets on different substrates. (A) A photo of as-grown BG on copper foil with a size of 5 cm×5 cm. (B) As-transferred BG sheets on several SiO₂/Si wafers. The letters “PSU” composed of BG can be obtained by tailoring the shape of PMMA-coated BG/Cu foils for transfer. (C) As-transferred BG on a quartz slide is highly transparent. (D-G) Scanning electron microscopy (SEM) images of BG sheets on Au TEM grid with different magnifications.

(3) Monolayer feature of as-synthesized BG sheets

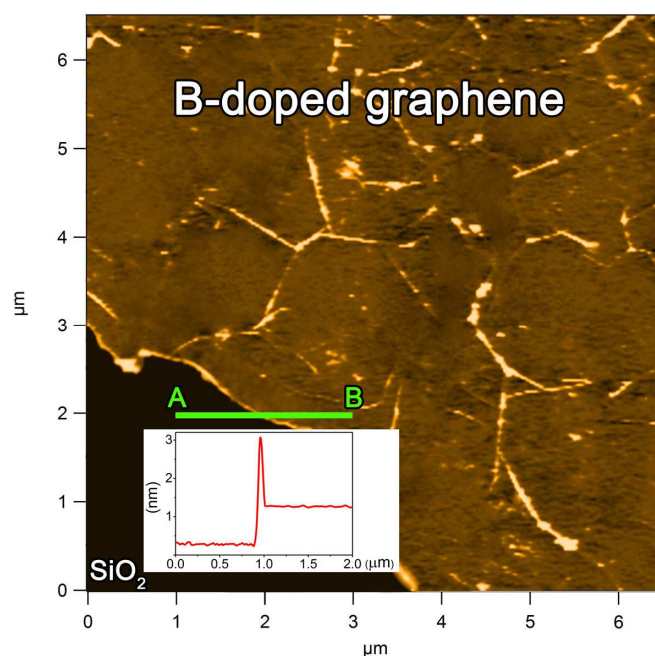


Fig. S4. Atomic force microscopy (AFM) analysis of BG sheets on a SiO₂/Si substrate. Inset is the corresponding height profile along the green line from A to B. The sharp peak might be caused by the PMMA residues located at the BG edges. It can be observed that the heights of BG are mostly around 0.98 nm, which can be regarded as a monolayer considering the substrate effect and surface adsorption (4).

(4) Grain size of as-synthesized BG sheets

To investigate the grain size of BG monolayer, we have carried out DF-TEM (dark-field transmission electron microscopy) observation following the literature (2). By this technique, it is possible to choose one of diffraction spots to create image. Fig. S5 and S6 show DF-TEM images from PG and BG, respectively. Due to the large size of the objective aperture, some spots are not fully separated. However, most of grains show clear boundaries, thus single grain can be easily distinguished. DF-TEM images revealed that both PG and BG are composed of grains ranging from ~ 100 nm to over $1 \mu\text{m}$. According to low magnification DF-TEM image from BG (Fig. S7), $\sim 7 \mu\text{m}$ of large domain was observed.

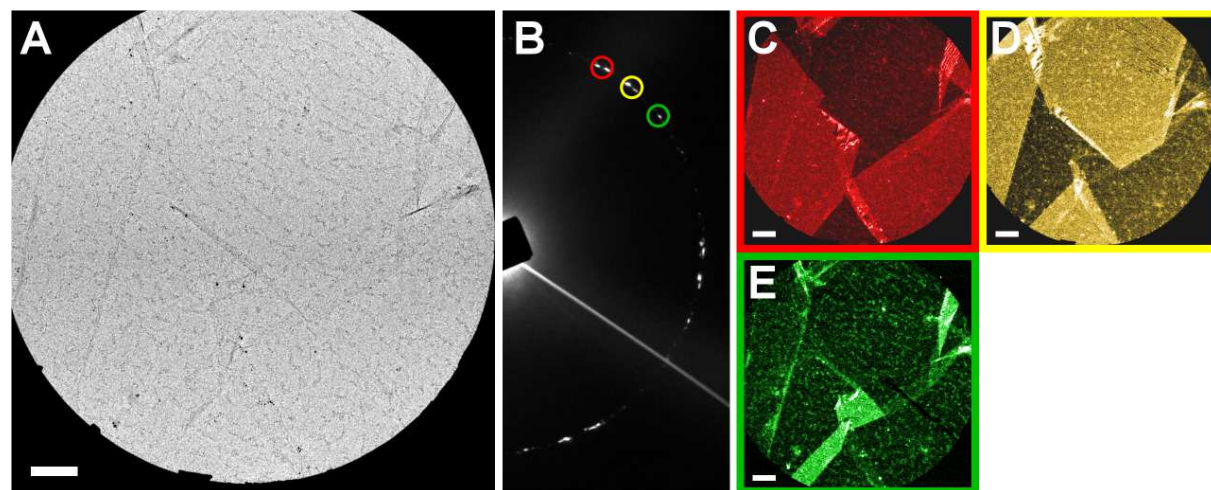


Fig. S5. DF-TEM analysis of PG. (A) Bright-field (BF) image of the area for analysis and (B) selected area electron diffraction (SAED) pattern for corresponding area. (C-E) False-colored dark-field (DF) image of the area, circled diffraction spots in SAED was used for DF-TEM imaging. The color of the border line corresponds to the circle in SAED of same color. Scale bar is $0.1 \mu\text{m}$.

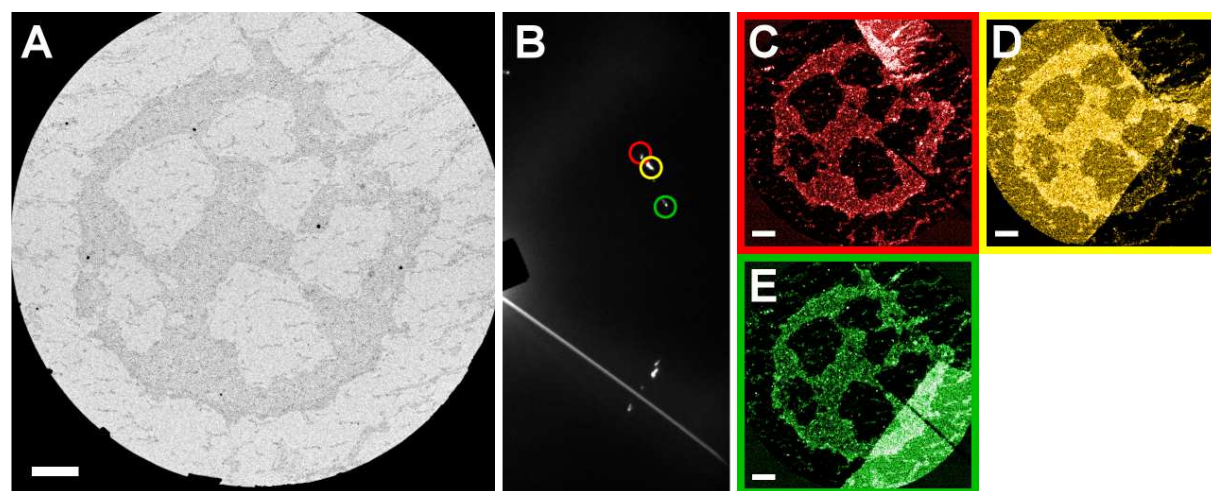


Fig. S6. DF-TEM analysis of BG. (A) Bright-field (BF) image of the area for analysis and (B) selected area electron diffraction (SAED) pattern for corresponding area. (C-E) False-colored Dark-field (DF) image of the area, circled diffraction spots in SAED was used for DF-TEM imaging. The color of the border line corresponds to the circle in SAED of same color. Scale bar is $0.1 \mu\text{m}$.

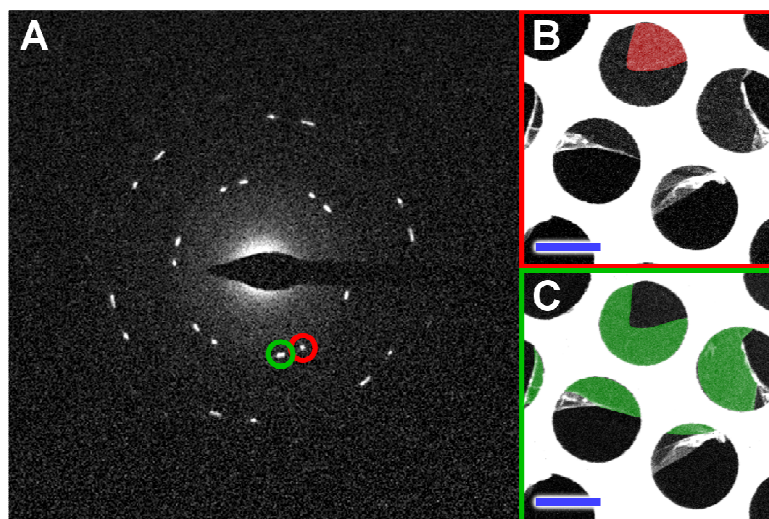


Fig. S7. Low magnification DF-TEM analysis of BG with larger grain size. (A) Selected area electron beam diffraction (SAED) pattern and (B-C) False-colored Dark-field (DF) images, circled diffraction spots in SAED was used for DF-TEM imaging. The white part in DF-TEM is amorphous carbon mesh of TEM grid. The color of the border line corresponds to the circle in SAED of same color. Scale bar is 2 μm .

(5) X-ray photoelectron spectroscopy (XPS) of BG sheets

XPS measurements were carried out using a Kratos AXIS Ultra with an Al $K\alpha$ X-ray source of 1486.6 eV and under a vacuum of 10^{-9} Torr. The XPS survey scan of freshly synthesized BG samples on copper foil substrates is shown in Fig. S8A. It can be observed that only peaks from B, C, Cu and O are detected, thus demonstrating that the freshly prepared CVD samples are free from contamination. Here B and C correspond to the graphene and Cu signals from the copper foil substrate, while the O peak might arise from the oxidation of the copper substrates after exposing it to the atmosphere. The atomic percentage of boron is $\sim 1.75\%$, which is calculated by the integrated intensity of the C1s and B1s narrow scan peak areas, considering their relative sensitivity factors (RSFs). Since there is no contamination for BG sheets, no other peaks (e.g. Cu) were considered in calculating the boron atomic percentage. We performed the calculations using RSFs of 1.000 for C and 0.486 for B. However, due to the atomic thickness of the BG sheet which is smaller than the electron inelastic mean free path, the signal will always show the substrate and thus only semiquantitative calculations are possible, i.e. the B/C atomic ratios.

The C1s fine scan analysis of BG sample is shown in Fig. S8B. For comparison, the C1s of PG sample is shown in Fig. S8C. Ideally, the C1s would change due to the presence of boron in the sample. However, the atomic abundance of B is less than 2 % of carbon, thus the C-B signal is relatively weak and too close to the C-C binding energy (ca. 285.3 eV). In addition, the intensity of the C 1s peak of graphene is relatively low, as expected from a monolayer material, thus all these combined factors make the accurate deconvolution of the C-B component very difficult, though a small increase of the full width at half maximum (FWHM) of the C1s peak can be seen. In our study, one can undoubtedly observe the presence of boron in the BG sample by analyzing the B1s spectra shown Fig. 1E.

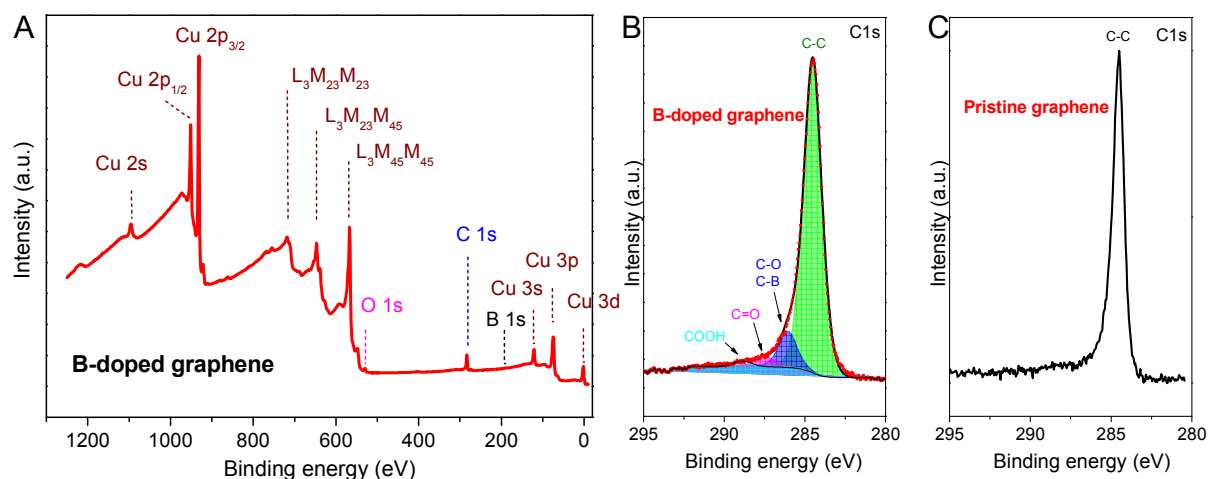


Fig. S8. (A) X-ray photoelectron spectroscopy (XPS) survey scan of BG sample on Cu foil substrate. The atomic percentage of B in as-synthesized BG sample is $\sim 1.75\%$. (B) and (C) are the C1s fine scans of BG and PG samples.

(6) Theoretical simulations of boron doping configurations

STM simulations were carried out within the Tersoff-Hamann approach-based density functional theory (DFT) by using a localized numerical basis set and norm-conserving pseudopotentials as implemented in the SIESTA package. *ab initio* DFT calculations were performed using the generalized gradient approximation (GGA) for the exchange correlation functional using norm conserving pseudo-potentials and a numerical localized combination of atomic orbitals to expand the wave-functions. The energy levels are populated using a Fermi-Dirac distribution with an electronic temperature of 250 K and an energy cutoff of 500 Ry is used. The supercell approach was used to treat defects, using at 10×10 to 16×16 unit cells. The integration over the 2D Brillouin zone is replaced by a summation over a Monkhorst-Pack (MP) grid of 8×8 k-points for 10×10 unit cells or equivalent kpoint density. The total and partial density of states were plotted using an interpolated 24×24 MP k-point grid, and smeared with Gaussian functions with a spread of 0.03 eV. The geometries are fully relaxed until the forces on each atom and stress tolerance are less than 0.01 eV/Å and 0.01 GPa, respectively. STM images were simulated using the Tersoff-Hamann approach, by integrating the local density of states within an energy window chosen to be close to the experimental bias. STS simulated curves were computed from the projected density of states (PDOS) close to the center of the complex of defects.

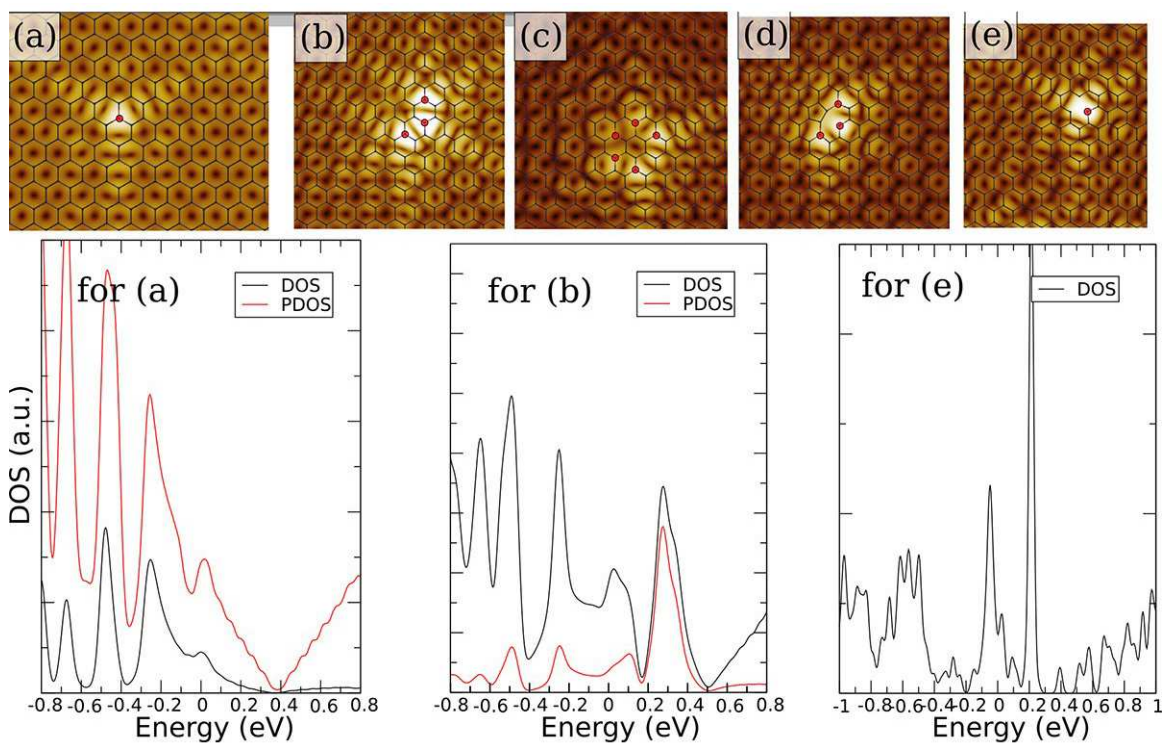


Fig. S9. Simulated STM and STS images for different B incorporations into graphene. Defects b, c, d, and e show the correct symmetry as that in Fig. 2B. However, only the STS of the defect shown in d exhibits the same signature as that depicted in Fig. 2E.

(7) Raman mapping analysis of BG sheets

Raman measurements were performed by a Renishaw inVia confocal micro-Raman spectrometer with a 100× objective and 514 nm laser as excitation source. For Raman mapping, the sample placed on an x - y piezo-stage and raster scanned with a step size of 400 nm for both x and y directions.

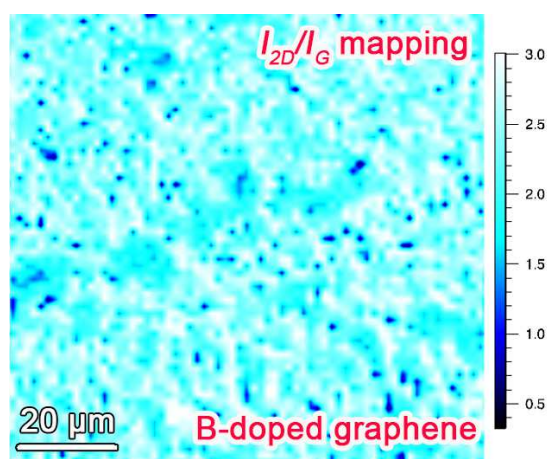


Fig. S10. Raman 2D-peak over G-peak intensity ratio (I_{2D}/I_G) mapping of BG on SiO_2/Si substrate.

(8) DFT analysis on enhanced gas sensing of BG sheets

The response of graphene to the presence of molecules has been investigated in the Ruitao Lv, *et al.*

literature (5). Two mechanisms have been proposed: one is based on the position of the LUMO of the absorbed molecule with respect to the Dirac point, another is the hybridization of the HOMO or LUMO orbitals with the π orbitals of graphene (5). For pristine graphene, NH_3 was found to be a donor, while NO_2 is an acceptor (5) with Hirshfeld charge transfer values of 0.027 and -0.099 electrons, respectively. In substitutional BG, NO_2 has been reported to exhibit an enhanced acceptor character with Lowdin charge transfer value of 0.350 electrons (6). In contrast, NH_3 molecules have been found only weakly bound to BG, exhibiting a distance to the plane of 3.37 Å (6). It should be pointed out that these works are based on GGA DFT calculations on rather small supercells of 4×4 (5, 6). In addition, it is often difficult to compare different population or charge distribution analysis methods, i.e., Hirshfeld versus Lowdin. For this reason, we have carried out DFT calculations using the KBM van der Waals functional as implemented in the SIESTA code in a 10×10 supercell using a $4\times 4\times 1$ k-point grid and 500 Ry for the mesh cutoff. Mulliken (similar to Lowdin), Hirshfeld, Voronoi and Bader population/charge analysis have been also computed. For pristine and single B substitution cases, we have started from the most stable positions found in previous works, and have further relaxed until the forces were less than $0.04 \text{ eV}/\text{Å}$. Spin-polarized calculations were also performed, however no magnetic moment was found. For the B_3 dopant model illustrated in Fig. 2 of our manuscript, no *a priori* position for the molecules can be considered. Therefore, a series of calculations were carried out for each of the two molecules. 12 sites were studied as depicted in Fig. S11. Total energy coarse calculations (i.e., 1 k-point 300 Ry.) calculations at fixed plane to molecule distance were used to find the three most stable sites for which full relaxation was performed. For all cases, the molecules tend to bind to the t_1 site.

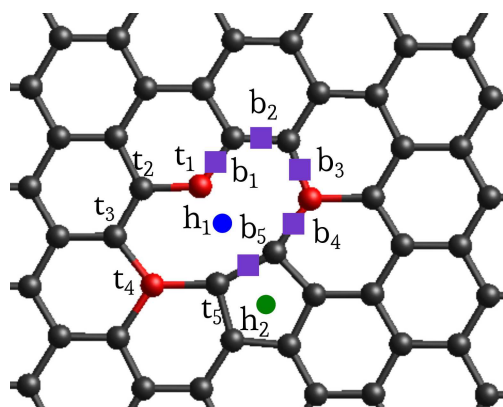


Fig. S11 Twelve possible binding sites ($t_1, t_2, t_3, t_4, t_5, b_1, b_2, b_3, b_4, b_5, h_1, h_2$) for the molecule on B_3 -doped graphene. The red and black balls represent boron and carbon atoms, respectively.

From the Bader charge analysis of Tables S1 and S2, the general donor and acceptor character of the NH_3 and NO_2 molecules, respectively, is confirmed. The charge and population analysis indeed predicts that BG demonstrates an opposite behavior between the

molecules and a larger change of sensitivity for NO₂ with respect to pristine graphene. Here, the Bader analysis is the most relevant, since we are interested in differences of charge transfer between different systems. However, this technique is widely recognized that it tends to overestimate the amount of charge transferred. Both Voronoi and Hirshfeld methods are two approaches based on geometrical partitions, thus offering a good counterweight for such an overestimation. From our DFT calculations, it can be safely concluded that B₃-doped graphene presents a better sensing behavior than pristine graphene because it exhibits a larger affinity to both donor and acceptor molecules, such as NH₃ and NO₂.

Table S1. Plane to molecule distance with N as reference (d) and charge and population analysis for NH₃ molecule on graphene, single B substitution (Gr-1B) and B₃ substitution (Gr-3B).

System	d (Å)	Mulliken	Hirshfeld	Voronoi	Bader
Gr-3B	3.0720(t1)	-0.0640	-0.0520	-0.0600	-0.2363
Gr-1B	3.3510(t)	0.7250	-0.0280	0.0040	-0.2014
Graphene	2.8900 (h)	-0.0190	0.0310	0.0340	-0.2243

Table S2. Plane to molecule distance with N as reference (d) and charge and population analysis for NO₂ molecule on graphene, single B substitution (Gr-1B) and B₃ substitution (Gr-3B).

System	d (Å)	Mulliken	Hirshfeld	Voronoi	Bader
Gr-3B	1.3770 (t1/h)	-0.2160	-0.0430	-0.0430	0.3196
Gr-1B	1.5630 (t)	0.0660	-0.1920	-0.3640	0.2282
Graphene	3.4330 (h)	0.2400	0.4580	-0.2370	-0.1826

Another theoretical work has recently suggested that screening of charged impurities may be another possible mechanism for conductance change in graphene gas sensing (7). Our *ab-initio* results reinforce this model due to significantly increased charge impurities which apparently make the screening more effective in BG samples. Due to the increased amount of defects caused by boron doping, we had observed 8-11 times reduced conductivity of BG devices compared to pristine graphene (PG) samples (Fig. S12). Because the sensitivity is proportional to the change of conductance divided by the baseline conductance, i.e., $\Delta G/G_0$, lowering G_0 will therefore inversely improve the device sensitivity.

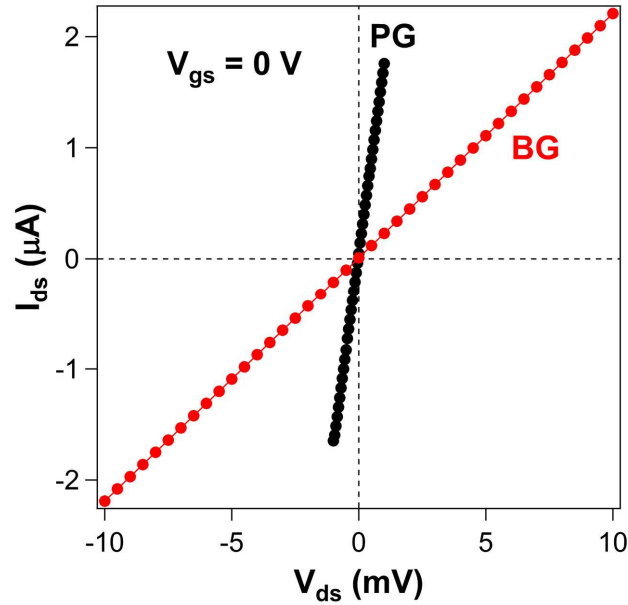


Fig. S12 I-V characteristics of BG and PG devices before UV light illumination

References:

1. Regan W, *et al.* (2010) A direct transfer of layer-area graphene. *Appl Phys Lett* 96(11):113102.
2. Huang PY, *et al.* (2011) Grains and grain boundaries in single-layer graphene atomic patchwork quilts. *Nature* 469(7330):389-392.
4. Zhu H, Xu Z, & Xie D (2011) *Graphene-Structure, Synthesis and Characterizations* (Tsinghua University Press, Beijing).
5. Leenaerts O, Partoens B, & Peeters FM (2008) Adsorption of H₂O, NH₃, CO, NO₂, and NO on graphene: A first-principles study. *Phys Rev B* 77(12):125416.
6. Dai JY, Yuan JM, & Giannozzi P (2009) Gas adsorption on graphene doped with B, N, Al, and S: A theoretical study. *Appl Phys Lett* 95(23):232105.
7. Liang S-Z, Chen G, Harutyunyan AR, & Sofo JO (2014) Screening of charged impurities as a possible mechanism for conductance change in graphene gas sensing. *Phys Rev B* 90(11):115410.